Self-Supervised Mutual Learning for Dynamic Scene Reconstruction of Spiking Camera

Shiyan Chen[1] , **Chaoteng Duan**[1] , **Zhaofei Yu**[2,3*] , **Ruiqin Xiong**[2] and **Tiejun Huang**[1,2,3]
[1]School of Electronic and Computer Engineering, Peking University
[2]School of Computer Science, Peking University
[3]Institute for Artificial Intelligence, Peking University
{strerichia002p,duanchaoteng}@stu.pku.edu.cn, {yuzf12,rqxiong,tjhuang}@pku.edu.cn

Abstract

Mimicking the sampling mechanism of the primate fovea, a retina-inspired vision sensor named spiking camera has been developed, which has shown great potential for capturing high-speed dynamic scenes with a sampling rate of 40,000 Hz. Unlike conventional digital cameras, the spiking camera continuously captures photons and outputs asynchronous binary spikes with various inter-spike intervals to record dynamic scenes. However, how to reconstruct dynamic scenes from asynchronous spike streams remains challenging. In this work, we propose a novel pretext task to build a self-supervised reconstruction framework for spiking cameras. Specifically, we utilize the blind-spot network commonly used in self-supervised denoising tasks as our backbone, and perform self-supervised learning by constructing proper pseudo-labels. In addition, in view of the poor scalability and insufficient information utilization of the blind-spot network, we present a mutual learning framework to improve the overall performance of the network through mutual distillation between a non-blind-spot network and a blind-spot network. This also enables the network to bypass constraints of the blind-spot network, allowing state-of-the-art modules to be used to further improve performance. The experimental results demonstrate that our methods evidently outperform previous unsupervised spiking camera reconstruction methods and achieve desirable results compared with supervised methods. The code is available at https://github.com/hnmizuho/SSML-Spiking-Camera-Reconstruction.

1 Introduction

High-speed imaging has been widely used in many fields, such as autonomous driving, industrial monitoring, and robotics. There has been a trade-off between speed and cost for conventional digital cameras. In order to capture high-speed moving objects, specialized sensors and shutters must be employed that are highly expensive, which impedes the popularization and further development of high-speed cameras. To address these issues, the spiking camera [Dong *et al.*, 2019; Dong *et al.*, 2017], a novel neuromorphic vision sensor, is invented for high-speed imaging with consumer-grade cameras. By abandoning the concept of exposure time, the spiking camera mimics the sampling mechanism of the primate fovea [Masland, 2012; Wässle, 2004], with each photosensitive unit continuously capturing photons independently and delivering spikes asynchronously when the accumulated intensity exceeds a given threshold, and achieves a time sampling frequency of 40,000 Hz. Different from another neuromorphic vision sensor called dynamic vision sensors (DVS)[Brandli *et al.*, 2014; Liu *et al.*, 2019; Huang *et al.*, 2017; Gallego *et al.*, 2022], which generates events only when the brightness change exceeds a certain threshold, the firing frequency of the output spike streams of spiking cameras is proportional to the received scene radiance. Therefore, the instantaneous light intensity can be inferred from the firing frequency, which allows the spiking camera to record more texture information than the event

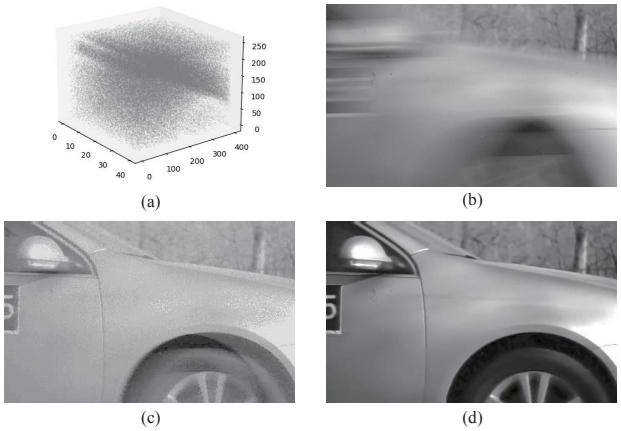

Figure 1: Illustrations of the spiking camera reconstruction task for a high speed car with a speed of 100 km/h. (a) Spike stream captured by a spiking camera. (b-d) Reconstructed images with TFP [Zhu *et al.*, 2019], STP [Zheng *et al.*, 2021] and our method. The proposed method achieves pleasant and high-quality result.

*Corresponding author

camera.

Despite these advantages, the asynchronous spike stream generated by spiking cameras is not friendly to the human visual system (Fig. 1a). It remains challenging to reconstruct dynamic scenes from asynchronous spike streams of the spiking camera. Generally, the reconstruction methods can be divided into internal statistics and deep learning methods. The internal statistics methods rebuild the scenes by estimating the firing frequency or firing interval of each pixel [Zhu *et al.*, 2019]. Although some recent methods have incorporated the mechanism of the retina system [Zhu *et al.*, 2020] and the short-term plasticity [Zheng *et al.*, 2021] to enhance the estimation of the firing frequency, it is hard to balance noise and motion blur. The deep learning methods utilize end-to-end convolutional neural networks to solve the reconstruction problem and achieve better performance than internal statistics approaches [Zhao *et al.*, 2021]. However, these methods rely on massive synthetic datasets with clean labels, while generating these datasets is still cumbersome and time-consuming. Additionally, the spiking camera suffers distinct noises under high and low light intensity [Zhu *et al.*, 2021], and the noise mechanisms have not been thoroughly investigated, which brings further challenges for the generation of the synthetic dataset.

In this work, we propose a novel pretext task to build a self-supervised reconstruction framework for spiking cameras, enabling us to train the network end-to-end on the real-world dataset without ground truth. Specifically, we utilize the blind-spot network commonly used in denoising tasks as our backbone and use simple internal statistics methods to construct pseudo-labels. In addition, we further excavate the potential of the blind-spot network in view of its poor scalability and insufficient information utilization, and present a mutual learning framework to improve the overall performance of the network through mutual distillation between a non-blind-spot network (NBSN) and a blind-spot network. As our NBSN is not hampered by any blind-spot constraints, state-of-the-art network architecture can be used to improve the performance. Moreover, we propose an adaptive motion inference module to obtain a better representation of the spiking data. We exploit various motion scales through temporal aggregation and inter-spike intervals [Zhu *et al.*, 2019], which allows the network to learn from better representations.

The main contributions are summarized as follows:

- We develop a self-supervised reconstruction framework for spiking cameras by constructing a novel pretext task. To the best of our knowledge, this is the first attempt to reconstruct dynamic scenes for spiking cameras via self-supervised learning without using a synthetic dataset.
- We propose an adaptive motion inference module to obtain a better representation for the spiking data.
- We present an effective mutual learning framework to improve the overall performance of the network. Besides, constraints of the blind-spot network can be bypassed in this approach.
- The proposed methods evidently outperform previous unsupervised methods, and achieve desirable results compared with supervised methods.

2 Related Work

Scene Reconstruction for Neuromorphic Vision Sensors. The event camera has shown distinctive potential in capturing high-speed and high-dynamic scenes. However, the event camera merely monitors the change of light intensity, making it challenging to record texture details in dynamic scenes [Zhao *et al.*, 2021]. Some recent studies [Choi *et al.*, 2020; Rebecq *et al.*, 2019a; Rebecq *et al.*, 2019b; Pini *et al.*, 2018] applied deep neural networks to reconstruct images directly from events, while others [Brandli *et al.*, 2014; Posch *et al.*, 2008] combined traditional images and events to obtain more texture information for reconstruction. Unlike event cameras, each photosensitive unit in the spiking camera accumulates photons independently and generates a spike when the dispatch threshold is reached. The higher the light intensity, the higher the spike frequency. This property enables the spiking camera to record rich texture information. The current main reconstruction methods are based on the temporal statistic characteristic of the spiking camera [Zhu *et al.*, 2019; Zhu *et al.*, 2020; Zheng *et al.*, 2021]. Zhu *et al.* [2019] presented two basic reconstruction methods, "texture from playback (TFP)" and "texture from inter-spike-intervals (TFI)", to rebuild the dynamic scenes from firing rate and firing interval, which requires careful choice of the window size to balance noise and motion blur. Some studies devoted to mimicking human physiological mechanisms, like retina-like visual imaging [Zhu *et al.*, 2020] and the short-term plasticity [Zheng *et al.*, 2021]. However, the reconstruction results of these bionic algorithms are noisy. Zhao *et al.* [2021] developed an end-to-end convolutional neural network and trained it on a synthetic dataset in a supervised way, which achieved state-of-the-art performance. Unfortunately, simulating large amounts of spike data is extremely challenging and expensive. Additionally, the noise mechanism of spike cameras has not been fully investigated. Thus the models trained with synthetic datasets suffer from the domain gap between synthetic and real noise.

Blind-Spot Network. Convolutional neural networks have achieved impressive performance in video denoising. However, supervised learning with large amounts of paired noisy-clean images in some areas, such as CT and MRI, can be costly and even unreachable. Therefore, researchers began to focus on self-supervised denoising. Lehtinen *et al.* [2020] trained the network with multiple independent noisy observations per scene. Further works proposed the blind-spot network (BSN) [Lehtinen *et al.*, 2018; Krull *et al.*, 2019; Laine *et al.*, 2019; Wu *et al.*, 2020; Byun *et al.*, 2021], which requires only one noisy observation per scene to train the network. Blind-spot means the network is designed to denoise each pixel from its surrounding spatial neighborhood without itself. Subsequent work improved the BSN by well-designed shifted convolutions [Laine *et al.*, 2019] and dilated convolutions [Wu *et al.*, 2020; Byun *et al.*, 2021]. However, these networks are carefully designed within the blind-spot constraints. Thus, some classic network modules, such as non-local attention and deformable convolution, cannot be employed directly into the network to improve performance. Huang et al. [2021] attempted to achieve self-supervised de-

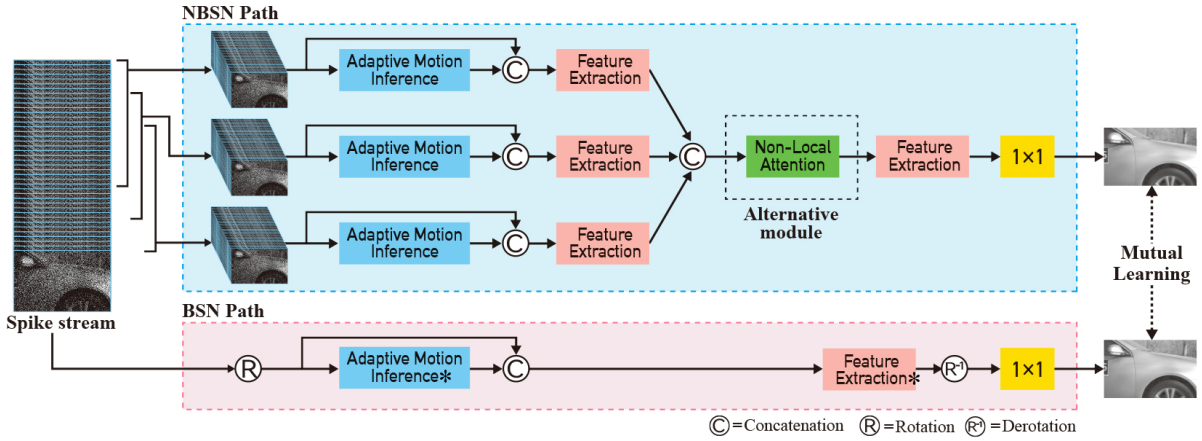

Figure 2: Illustration of the proposed self-supervised mutual learning framework for dynamic scene reconstruction. The BSN and NBSN serve as two students in mutual learning, and transfer useful knowledge to each other. The NBSN also bypasses the blind-spot restrictions and enables state-of-the-art modules, e.g. non-local attention module in the green box, to be added to improve performance. Module with '*' means shifted-convolution is used in it.

noising without modifying the network, and can enjoy the progress of state-of-the-art network architecture design.

Mutual Learning. Knowledge distillation [Hinton *et al.*, 2015] is a pioneering work to transfer knowledge from strong teacher networks to student networks. Recently, a variant of the knowledge distillation method called mutual learning [Zhang *et al.*, 2018] has been proposed, breaking the "teacher-student" structure and advocating collaborative learning between a group of student networks. While most knowledge distillation methods focus on classification tasks, some methods suitable for regression tasks have been proposed [Peng *et al.*, 2021; Wang *et al.*, 2021; Wu *et al.*, 2020]. In this paper, we apply the knowledge distillation for reconstruction tasks, more precisely, we present an effective mutual learning framework where a non-blind-spot network and a blind-spot network can learn from each other.

3 Methods

In this section, we first formulate the mechanism of the spiking camera, then present the whole reconstruction framework and the mutual learning strategy.

3.1 Spiking Camera

Working Mechanism

Spiking camera is composed of an $H \times W$ array of pixels, with each pixel independently accumulating the incoming light intensity $L(t)$ persistently. When the instantaneous electric charge amount $A(t)$ on the integrator reaches a dispatch threshold θ, a spike is fired, and then the integrator is reset to 0. The relationship between $L(t)$ and $A(t)$ is formulated as:

$$A(t) = \int_0^t \alpha \cdot L(x)\mathrm{d}x \mod \theta, \tag{1}$$

where α is the photoelectric conversion rate.

Although spikes can fire at arbitrary time t_k given $A(t_k) = 0$, it can only be read out by checking the spike flag at discrete times due to the limitations of circuit technology. Specially, the camera checks the spike flag periodically with a fixed interval $T = 25$ μs. A spike will be read out $S(n) = 1$ $(n = 1, 2, \ldots)$ if the spike flag has been set up at the time t, with $(n-1)T < t \leqslant nT$. Otherwise it reads out $S(n) = 0$. Considering that all the pixels on the sensor continuously accumulate the incoming light and fire spikes independently, the spiking camera would produce a continuous binary spike stream $S \in \{0,1\}^{H\times W\times N}$ during the period $[0, NT]$.

Basic Reconstruction Methods

The goal of scene reconstruction of the spiking camera is to restore the intensity images $\{I_n | I_n \in [0,255]^{H\times W}, n = 1, 2, \ldots N\}$ from the output spike stream $S \in \{0,1\}^{H\times W\times N}$. The basic reconstruction methods are "texture from play-back (TFP)" and "texture from inter-spike-intervals (TFI)" [Zhu *et al.*, 2019], utilizing that the photosensitive units of spiking camera receive different scene radiance will trigger spikes with different frequencies.

The TFP method obtains the pixel value by calculating the number of spikes in a time window, which is formulated as:

$$I_n^{\mathrm{TFP}} = \frac{N_w}{w} \cdot C, \tag{2}$$

where I_n^{TFP} refers to the pixel value at moment n, w is the size of time window, N_w is the total number of spikes collected in the time window, and the C refers to the maximum dynamic range of the reconstruction.

The TFI method assumes that the scene radiance $L(t)$ is a constant $\overline{L}$ in a short period. According to Eq. 1, the spike generation can be simplified as $\overline{L}\Delta t \geq \theta$, where Δt is the inter-spike interval (ISI) obtained by calculating the time between two neighboring spikes. Thus, the pixel value can be estimated with two spikes:

$$I_n^{\mathrm{TFI}} = \frac{C}{\Delta t_n}, \tag{3}$$

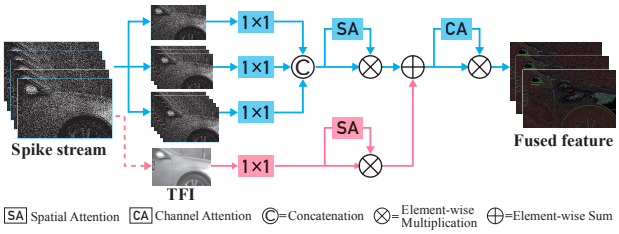

Figure 3: The proposed adaptive motion inference module (AMIM). The network obtains the information of static region and moving region from TFP path and TFI path respectively, and then fuse them adaptively through attention block.

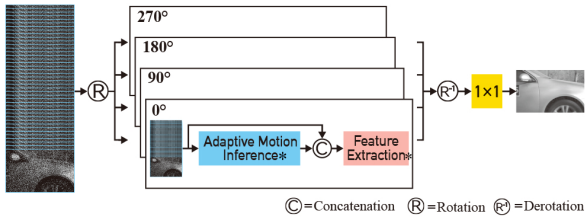

Figure 4: Detailed architecture of the BSN path in Fig. 2. Module with '*' means shifted-convolution is used in it.

where Δt_n represents the ISI corresponding to moment n.

3.2 Self-Supervised Reconstruction Network

Overview Architecture

In this section, we propose the self-supervised reconstruction framework. The overall network structure is illustrated in Fig. 2, which takes a consecutive spike stream $S \in \{0,1\}^{H\times W\times N}$ as input. The network consists of two reconstruction paths, one is a blind-spot network (BSN), and the other is a non-blind-spot network (NBSN), i.e. an unprocessed conventional convolutional neural network. The NBSN path process the input stream in a two-stage manner commonly used in video processing [Sheth *et al.*, 2021; Tassano *et al.*, 2020]. In the first stage, the input spike stream is split into three overlapping sub-stream $\{S_{t-k}, S_t, S_{t+k}\}$, where S_t denotes the sub-stream around time t and k denotes the overlap size. Next, each sub-stream goes through the Adaptive Motion Inference Module, producing coarse estimation features $\{F_{t-k}, F_t, F_{t+k}\}$ under attention weighting. Then each concatenation of the estimation features and the sub-stream is sent to the Feature Extraction Module (a modified share-weight U-Net) to extract further features $\{\hat{F}_{t-k}, \hat{F}_t, \hat{F}_{t+k}\}$. In the second stage, a Non-Local Attention Module is applied to fuse these features to strengthen feature representations. Finally, the fused features are sent to another modified U-Net followed by 1×1 convolutions to reconstruct the final clean image $\hat{I}_t$. The working flow of the BSN path follows a one-stage manner. Specifically, the input spike stream is fed into the Adaptive Motion Inference Module directly, then a modified U-Net followed by 1×1 convolutions is applied to the concatenated output to produce the final reconstruction result. The two paths are jointly trained using mutual learning paradigm.

Adaptive Motion Inference Module (AMIM)

A continuous spike stream contains multiple spike frames, which provide rich information to reconstruct the high-quality image. However, because of the complexity of the motion scene, extracting appropriate features remains challenging. Inspired by the fact that TFI and TFP methods are suitable for dealing with moving and stationary scenes respectively[Zhu *et al.*, 2019], we propose an attention-based AMIM to extract more valuable features from these two basic reconstruction methods (Fig. 3). First, in the stationary branch, three sets of masks and 1×1 convolutions are used to perform multi-scale temporal aggregation imitating the process of TFP:

$$F_{t_i}^1 = f_{t_i}^1(M_i^1 \circ S_t^1), \quad i = 1,2,3, \tag{4}$$

where M_i^1 is the mask of the i-th scale, $f_{t_i}^1$ denotes the corresponding 1×1 convolution and $\circ$ denotes element-wise multiplication. Then a spatial attention block $M_s^1(\cdot)$ is used on the concatenated output to find the stationary area.

$$\hat{F}_t^1 = M_s^1([F_{t1}^1, F_{t2}^1, F_{t3}^1]), \tag{5}$$

where $[,]$ denotes feature concatenation.

Second, in the motion path, the TFI reconstruct I_t^{TFI} is fed into a 1×1 convolution $f_t^2(\cdot)$ and spatial attention block $M_s^2(\cdot)$ to find the motion area.

$$\hat{F}_t^2 = M_s^2(f_t^2(I_t^{\text{TFI}})). \tag{6}$$

Finally, a channel attention block M_c is introduced to obtain the final fused features $\hat{F}_t$:

$$\hat{F}_t = M_c(\hat{F}_t^1 \oplus \hat{F}_t^2), \tag{7}$$

where $\oplus$ denotes the element-wise sum.

Pretext Task Using Blind-Spot Network

We build the BSN framework using the blind-spot strategy proposed in [Laine *et al.*, 2019] to estimate each output pixel from a spatio-temporal neighborhood without the pixel itself. The training of the BSN does not require noisy-clean image pairs. Instead, it utilizes the noisy image itself as both input and supervision signals.The blind-spot constraint will prevent the network from learning identity mapping to noisy images, but produce clean results. These motivate us to use BSN as our backbone to achieve self-supervision and clean output. A natural idea is to use noisy TFI (or TFP) as both input and supervision signal, while in order to fully mine the rich temporal information of spike stream, we take the spike stream as the input.

In our BSN framework (Fig. 4), the rotated versions of the input spike stream are concatenated together in the batch dimension. Then we pass the input through the shifted-conv based BSN, leading to an output with four times the number of batch-size. After that, the output reverts into four parts in the batch dimension and concatenated together in the channel dimension, and finally passes through 1×1 convolutions to produce the estimated reconstruction image $\hat{I}_t^{bsn}$.

We use the self-supervised denoising task as a pretext task to train the network. We hope that the BSN can remove the

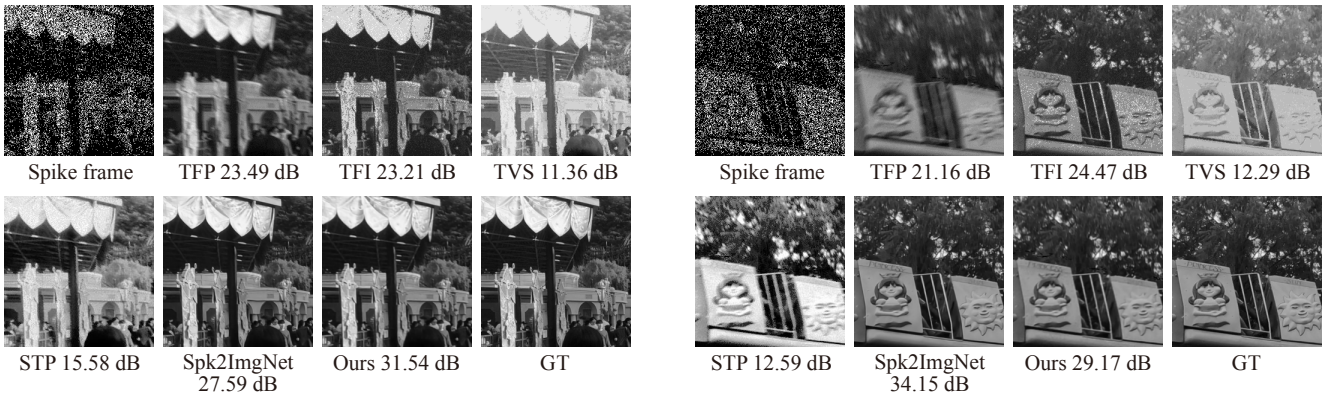

Figure 5: Evaluation of different methods on synthetic dataset.

noise and improve the details of the latent image in the spike stream, so as to output high-quality noiseless reconstruction images. In order to train the network reasonably and effectively, it is necessary to find appropriate pseudo-labels for self-supervision. As discussed in Sec. 3.1, we can utilize simple internal statistics results, such as TFI or TFP as the noisy label to train the network. We refer to the pseudo-label as I_{pseudo}, and the reconstruction loss function can be formulated as:

$$\mathcal{L}_{rec} = \|\hat{I}_t^{bsn} - I_{pseudo}\|_2^2. \tag{8}$$

The use of the BSN ensures that the network trained with TFI (or TFP) as pseudo-labels will not learn to reconstruct labels themselves, but learn their latent clean representations.

Mutual Learning Strategy

The BSN framework faces the following problems:

- The blind-spot network relies heavily on specific convolution kernel design, which leads to poor network scalability. Thus the state-of-the-art modules in supervised learning can not be applied to the network directly.
- The nature of the blind-spot makes it impossible for each pixel of the output to obtain information from the corresponding position of the input, which reduces the utilization of information by the network compared to normal CNNs.
- The rotation operation makes the input batch-size quadruple the original size. Besides, due to the overlapped receptive fields of different rotation versions, the input pixels are processed twice, resulting in redundant calculation and a high inference cost.

Among them, the first two are common problems of most blind-spot networks [Krull *et al.*, 2019; Laine *et al.*, 2019; Wu *et al.*, 2020; Byun *et al.*, 2021], and the third is unique to the network we use in Sec. 3.2

To address these issues, we propose a mutual learning paradigm between the BSN and the NBSN. As the NBSN is a normal convolution network, we can add modules popular in supervised learning without limitations. In this paper we use a separated non-local attention module (green box in Fig. 2) [Huang *et al.*, 2019; Fu *et al.*, 2019; Wang *et al.*, 2018]. Specifically, criss-cross spatial attention [Huang *et al.*, 2019], channel attention, and temporal attention are applied to the concatenated feature of the outputs of first stage separately to exploit the long-term temporal correlation.

In our mutual learning framework, both BSN and NBSN can be regarded as "student network", while learning collaboratively and implicitly transfer useful knowledge to each other. The BSN provides the NBSN with "clean" features learned by the blind-spot strategy, meanwhile, the NBSN, as a "stronger student" with more temporal correlation information and powerful modules, promotes the BSN with more refined information. For the classification tasks, KL-divergence is used as mutual learning loss to utilize soft labels for knowledge transfer [Zhang *et al.*, 2018]. For the regression task, we define the mutual learning loss function as

$$\mathcal{L}_{mutual} = \|\hat{I}_t^{nbsn} - \hat{I}_t^{bsn}\|_2^2, \tag{9}$$

and the total loss function can be formulated as

$$\mathcal{L}_{total} = \mathcal{L}_{rec} + \lambda \mathcal{L}_{mutual}, \tag{10}$$

where λ is a weighting parameter. After training, we only use the NBSN path to produce reconstruction images, thus the high computational cost of the BSN path can be avoided.

4 Experiments

We evaluate the performance of our method on both synthetic and real-world datasets.

4.1 Evaluation on Synthetic Dataset

Synthetic Dataset

For quantitative evaluation, we use the synthetic dataset with ground truth to train our network, which is obtained from SpkImgNet [Zhao *et al.*, 2021]. This synthetic dataset is generated by converting videos from REDS [Nah *et al.*, 2019] to spike stream, with frames in the videos as the ground truth. The training set consists of 800 spike stream-ground truth pairs with a spatial resolution of 400×250, and the testing set consists of 40 spike stream-ground truth pairs of the same size. We compare our method with previous representative reconstruction works, including TFI and TFP [Zhu *et al.*, 2019], TVS [Zhu *et al.*, 2020], STP [Zheng *et al.*, 2021] and Spk2ImgNet [Zhao *et al.*, 2021].

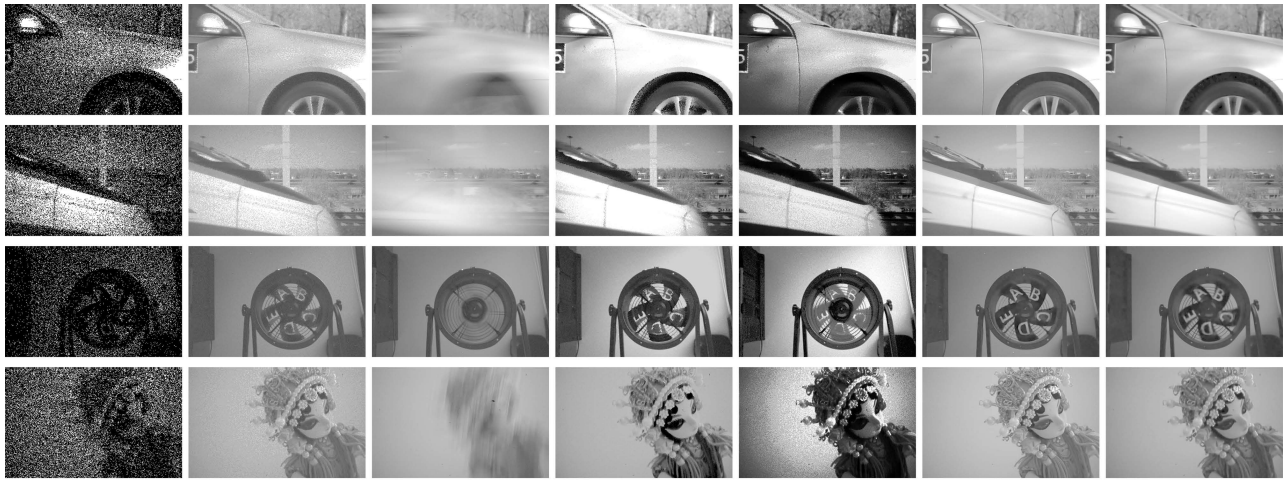

(a) Spike frame (b) TFI (c) TFP (d) TVS (e) STP (f) Spike2ImgNet (g) Ours

Figure 6: Reconstruction results on real-world dataset.

Methods	Supervised	Unsurpervised				
	Spk2ImgNet	TFI	TFP	TVS	STP	Ours
PSNR	**38.44**	24.94	22.37	23.15	22.37	**34.26**
SSIM	**0.9767**	0.7150	0.5801	0.7452	0.7300	**0.9718**

Table 1: Comparison among different reconstruction methods on synthetic dataset. Red: best. Blue: second.

Scene	Sample rate	Resolution	Description
Car	20,000 Hz	400 × 250	100 km/h
Doll	20,000 Hz	400 × 250	Free fall
Fan	40,000 Hz	400 × 250	2600 rpm
Train	20,000 Hz	400 × 250	350 km/h

Table 2: Details of real-world dataset.

Methods	Supervised	Unsurpervised				
	Spk2ImgNet	TFP	TFI	TVS	STP	Ours
Car	**4.0028**	7.6423	13.0197	9.3054	5.5144	**3.7595**
Doll	**3.9737**	8.2026	7.9594	7.4768	7.3340	**5.3591**
Fan	**3.7233**	7.2340	11.9794	6.2319	4.6580	**4.5007**
Train	**3.7140**	6.4892	10.6230	6.7824	5.1873	**3.6053**
Average	**3.8532**	7.3920	10.8954	7.4491	5.6734	**4.3061**

Table 3: Comparison of NIQE (↓) on real-world dataset.

Methods	PSNR	SSIM
BSN	32.96	0.9604
BSN+AMIM	**33.23**	**0.9635**
BSN+AMIM+LTC	28.25	0.9102
BSN+AMIM+LTC+NLA	25.45	0.8106

Table 4: Ablation study for a single BSN without mutual learning.

Qualitative and Quantitative Evaluation

Here PSNR and SSIM are used to compare our method with previous methods quantitatively. As illustrated in Tab. 1, our method outperforms the previous unsupervised methods evidently. The performance of our method is slighter lower than Spk2ImgNet. However, as a supervised method, the training of Spk2ImgNet depends on a large synthetic dataset with ground truth, and generating the dataset through a spike simulator is a cumbersome and time-consuming task. In contrast, our self-supervision method can be trained directly on the real world dataset, which can be easily obtained by the spiking camera. The reconstruction results of compared methods are illustrated in Fig. 5.

4.2 Evaluation on Real World Dataset

We also compare our methods with the state-of-the-art methods on real-world dataset captured by the spiking camera with a sampling rate of 40,000 Hz. This dataset consists of four different sequences, including high-speed scenes with the object's motion and high-speed scenes with the camera's ego-motion, such as a rotating fan with 2600 rpm (revolutions per minute) and high-speed trains in 350 km/h, etc. Please refer to Table. 2 for more information.

As shown in Fig. 6, our method achieves better performance than the unsupervised methods. Specifically, the TFP method suffers from severe motion blur under larger window size, and appears to be noisy under smaller window sizes. The TFI, TVS and the STP-based method can restore the motion area effectively, while the appearance of noise can not be ignored. Furthermore, our method has achieved almost the same qualitative performance as the supervised method, with clean textures and rich details. Similar to Spk2ImgNet, we use a no-reference image quality assessment metric named NIQE to evaluate the performance of different scenes on the real-world dataset. As shown in Tab. 3, our method outperforms previous unsupervised reconstruction methods and achieves comparable performance to the supervised method.

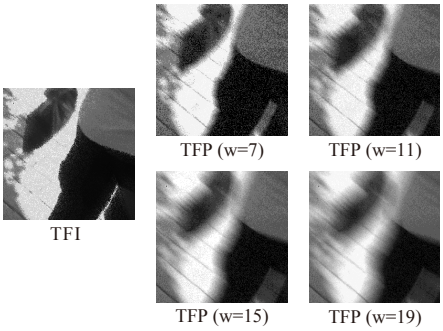

Figure 7: Illustrations of different pseudo-labels.

Methods	PSNR	SSIM
BSN & NBSN	33.83	0.9680
BSN & NBSN+LTC	34.01	0.9701
BSN & NBSN+LTC+NLA	**34.26**	**0.9718**

Table 5: Ablation study for different network configurations of the two student network in mutual learning.

4.3 Ablation Study

Reconstruction without Mutual Learning

In this section, we explore the effect of the proposed modules and demonstrate the limitations of a single BSN through experiments on the synthetic dataset. The experiments are conducted in a single BSN. Specifically, the mutual learning strategy is not used. As shown in Table 4, a single BSN with the proposed AMIM module performs best, indicating that the proposed AMIM can provide a better representation for spike stream through adaptive motion inference. Besides, we notice that BSN with long-term temporal correlation (LTC) does not show the expected performance, which we attribute to the lack of explicit temporal fusion.

Moreover, BSN with LTC and a non-local attention (NLA) module performs poorly. It is because the non-local nature of this module breaks the blind-spot constraint that an output pixel can only obtain information from its surrounding spatial neighborhood without itself. With these experiments, we have demonstrated the poor scalability of a single BSN without mutual learning. As BSN with LTC and NLA breaks the blind-spot constraint of the denoising pretext task, these results can also be regarded as ablation for the pretext task.

Reconstruction with Mutual Learning

We further evaluate the effect of different network configurations of the two student networks in mutual learning. Note that the AMIM module is employed in all networks listed in the Tab. 5 in order to reduce unnecessary experiments. As shown in Tab. 5, the combination of an NBSN with LTC followed by a NLA module and a BSN with only short-term temporal correlation performs best, which outperforms the best network in Tab. 4 by around 1 dB. It indicates that our mutual learning strategy can transfer valuable knowledge to each other to improve performance.

Pseudo-Labels	PSNR	SSIM
TFI	33.09	0.9605
TFP($w = 7$)	34.19	0.9713
TFP($w = 11$)	33.94	0.9695
TFP($w = 15$)	33.41	0.9657
TFP($w = 19$)	32.81	0.9599

Table 6: Ablation study for the effect of different pseudo-labels on the synthetic dataset.

We also notice that even the simple combination of a BSN and NBSN with the same structure can achieve better performance than a single BSN, and the performance will improve with the addition of more modules in the NBSN, which implies that the poor scalability of BSN can also be bypassed through our mutual learning strategy.

Effect of Different Pseudo-Labels

Table. 6 shows the performance trained with different pseudo-labels on the proposed network. Note that the performance decreases as windows grow, as larger windows may introduce more motion blur, which can be seen in Fig. 7.

4.4 Implementation Details

The parameter λ of the loss function is set to 0.01, and the input spike stream is cropped into 40×40 patches with a batch size of 4. Besides, we set the short-term temporal window size and long-term temporal window size to 41 and 27, respectively, and remove all additive terms from the convolutional layer as in [Sheth *et al.*, 2021] for better generalization. Moreover, we use Adam optimizer with the default setting to optimize our network, and train the network with TFP ($w = 7$) as pseudo labels on Nvidia RTX 2080 GPU for 100k iterations. The BSN path is first trained for 15k iterations before mutual learning.

5 Conclusions

In this paper, we present an end-to-end self-supervised mutual learning framework to address the reconstruction problem of the spiking camera. We adopt the blind-spot network into the reconstruction problem and construct a proper self-supervised pseudo-label by utilizing the two basic reconstruction methods, TFI and TFP. To overcome the limitations of the blind-spot network, we propose a mutual learning strategy for knowledge transfer between a non-blind-spot network and a blind-spot network. Experiments on both synthetic and real-world datasets have demonstrated that the proposed framework can restore pleasant and high-quality images from spike streams and achieve comparable results as the supervised method. To the best of our knowledge, this is the first attempt to restore dynamic scenes from the spiking camera in a self-supervised manner without using any synthetic dataset.

Acknowledgments

This work was supported by the National Key Research and Development Program of China (Grant No.2021ZD0200300) and the National Natural Science Foundation of China (Grant No.62176003 and No.62088102).

References

[Brandli *et al.*, 2014] Christian Brandli, Raphael Berner, Minhao Yang, Shih-Chii Liu, and Tobi Delbruck. A 240× 180 130 db 3 μs latency global shutter spatiotemporal vision sensor. *IEEE Journal of Solid-State Circuits*, 49(10):2333–2341, 2014.

[Byun *et al.*, 2021] Jaeseok Byun, Sungmin Cha, and Taesup Moon. FBI-Denoiser: Fast blind image denoiser for poisson-gaussian noise. In *CVPR*, pages 5768–5777, 2021.

[Choi *et al.*, 2020] Jonghyun Choi, Kuk-Jin Yoon, et al. Learning to super resolve intensity images from events. In *CVPR*, pages 2768–2776, 2020.

[Dong *et al.*, 2017] Siwei Dong, Tiejun Huang, and Yonghong Tian. Spike camera and its coding methods. *DCC*, 2017.

[Dong *et al.*, 2019] Siwei Dong, Lin Zhu, Daoyuan Xu, Yonghong Tian, and Tiejun Huang. An efficient coding method for spike camera using inter-spike intervals. *DCC*, 2019.

[Fu *et al.*, 2019] Jun Fu, Jing Liu, Haijie Tian, Yong Li, Yongjun Bao, Zhiwei Fang, and Hanqing Lu. Dual attention network for scene segmentation. In *CVPR*, pages 3146–3154, 2019.

[Gallego *et al.*, 2022] Guillermo Gallego, Tobi Delbrück, Garrick Orchard, Chiara Bartolozzi, Brian Taba, et al. Event-based vision: A survey. *IEEE Transactions on PAMI*, 44(1):154–180, 2022.

[Hinton *et al.*, 2015] Geoffrey Hinton, Oriol Vinyals, and Jeff Dean. Distilling the knowledge in a neural network. *arXiv preprint arXiv:1503.02531*, 2015.

[Huang *et al.*, 2017] Jing Huang, Menghan Guo, and Shoushun Chen. A dynamic vision sensor with direct logarithmic output and full-frame picture-on-demand. In *ISCAS*, pages 1–4, 2017.

[Huang *et al.*, 2019] Zilong Huang, Xinggang Wang, Lichao Huang, Chang Huang, Yunchao Wei, and Wenyu Liu. Ccnet: Criss-cross attention for semantic segmentation. In *ICCV*, pages 603–612, 2019.

[Huang *et al.*, 2021] Tao Huang, Songjiang Li, Xu Jia, Huchuan Lu, and Jianzhuang Liu. Neighbor2neighbor: Self-supervised denoising from single noisy images. In *CVPR*, pages 14781–14790, 2021.

[Krull *et al.*, 2019] Alexander Krull, Tim-Oliver Buchholz, and Florian Jug. Noise2void-learning denoising from single noisy images. In *CVPR*, pages 2129–2137, 2019.

[Laine *et al.*, 2019] Samuli Laine, Tero Karras, Jaakko Lehtinen, and Timo Aila. High-quality self-supervised deep image denoising. *NeurIPS*, 32:6970–6980, 2019.

[Lehtinen *et al.*, 2018] Jaakko Lehtinen, Jacob Munkberg, Jon Hasselgren, Samuli Laine, Tero Karras, Miika Aittala, and Timo Aila. Noise2noise: Learning image restoration without clean data. In *ICML*, pages 2971–2980, 2018.

[Liu *et al.*, 2019] Shih-Chii Liu, Bodo Rueckauer, Enea Ceolini, Adrian Huber, and Tobi Delbruck. Event-driven sensing for efficient perception: Vision and audition algorithms. *IEEE Signal Processing Magazine*, 36(6):29–37, 2019.

[Masland, 2012] Richard H Masland. The neuronal organization of the retina. *Neuron*, 76(2):266–280, 2012.

[Nah *et al.*, 2019] Seungjun Nah, Sungyong Baik, Seokil Hong, Gyeongsik Moon, Sanghyun Son, Radu Timofte, and Kyoung Mu Lee. Ntire 2019 challenge on video deblurring and super-resolution: Dataset and study. In *CVPR Workshops*, pages 0–0, 2019.

[Peng *et al.*, 2021] Rui Peng, Ronggang Wang, Yawen Lai, Luyang Tang, and Yangang Cai. Excavating the potential capacity of self-supervised monocular depth estimation. In *ICCV*, pages 15560–15569, 2021.

[Pini *et al.*, 2018] Stefano Pini, Guido Borghi, and Roberto Vezzani. Learn to see by events: Color frame synthesis from event and rgb cameras. *arXiv preprint arXiv:1812.02041*, 2018.

[Posch *et al.*, 2008] Christoph Posch, Daniel Matolin, and Rainer Wohlgenannt. An asynchronous time-based image sensor. In *ISCAS*, pages 2130–2133, 2008.

[Rebecq *et al.*, 2019a] Henri Rebecq, René Ranftl, Vladlen Koltun, and Davide Scaramuzza. Events-to-video: Bringing modern computer vision to event cameras. In *CVPR*, pages 3857–3866, 2019.

[Rebecq *et al.*, 2019b] Henri Rebecq, René Ranftl, Vladlen Koltun, and Davide Scaramuzza. High speed and high dynamic range video with an event camera. *IEEE Transactions on PAMI*, 2019.

[Sheth *et al.*, 2021] Dev Yashpal Sheth, Sreyas Mohan, Joshua L Vincent, Ramon Manzorro, Peter A Crozier, Mitesh M Khapra, Eero P Simoncelli, and Carlos Fernandez-Granda. Unsupervised deep video denoising. In *ICCV*, pages 1759–1768, 2021.

[Tassano *et al.*, 2020] Matias Tassano, Julie Delon, and Thomas Veit. Fastdvdnet: Towards real-time deep video denoising without flow estimation. In *CVPR*, pages 1354–1363, 2020.

[Wang *et al.*, 2018] Xiaolong Wang, Ross Girshick, Abhinav Gupta, and Kaiming He. Non-local neural networks. In *CVPR*, pages 7794–7803, 2018.

[Wang *et al.*, 2021] Yanbo Wang, Shaohui Lin, Yanyun Qu, Haiyan Wu, Zhizhong Zhang, Yuan Xie, and Angela Yao. Towards compact single image super-resolution via contrastive self-distillation. In *IJCAI*, pages 1122–1128, 2021.

[Wässle, 2004] Heinz Wässle. Parallel processing in the mammalian retina. *Nature Reviews Neuroscience*, 5(10):747–757, 2004.

[Wu *et al.*, 2020] Xiaohe Wu, Ming Liu, Yue Cao, Dongwei Ren, and Wangmeng Zuo. Unpaired learning of deep image denoising. In *ECCV*, pages 352–368. Springer, 2020.

[Zhang *et al.*, 2018] Ying Zhang, Tao Xiang, Timothy M Hospedales, and Huchuan Lu. Deep mutual learning. In *CVPR*, pages 4320–4328, 2018.

[Zhao *et al.*, 2021] Jing Zhao, Ruiqin Xiong, Hangfan Liu, Jian Zhang, and Tiejun Huang. Spk2imgnet: Learning to reconstruct dynamic scene from continuous spike stream. In *CVPR*, pages 11996–12005, 2021.

[Zheng *et al.*, 2021] Yajing Zheng, Lingxiao Zheng, Zhaofei Yu, Boxin Shi, Yonghong Tian, and Tiejun Huang. High-speed image reconstruction through short-term plasticity for spiking cameras. In *CVPR*, pages 6358–6367, 2021.

[Zhu *et al.*, 2019] Lin Zhu, Siwei Dong, Tiejun Huang, and Yonghong Tian. A retina-inspired sampling method for visual texture reconstruction. In *ICME*, pages 1432–1437. IEEE, 2019.

[Zhu *et al.*, 2020] Lin Zhu, Siwei Dong, Jianing Li, Tiejun Huang, and Yonghong Tian. Retina-like visual image reconstruction via spiking neural model. In *CVPR*, pages 1438–1446, 2020.

[Zhu *et al.*, 2021] Lin Zhu, Jianing Li, Xiao Wang, Tiejun Huang, and Yonghong Tian. Neuspike-net: High speed video reconstruction via bio-inspired neuromorphic cameras. In *ICCV*, pages 2400–2409, 2021.